Morphological Changes in Composite-Based Organic Light-Emitting Diodes

Helmut Hänsel,[†] David C. Müller,[‡,§] Markus Gross,[‡,⊥] Klaus Meerholz,[‡,§] and Georg Krausch*[,†]

Institut für Physikalische Chemie, Universität Bayreuth, D-95440 Bayreuth, Germany, and Department Chemie, Universität München, Butenandtstr. 11, D-81377 München, Germany

Received December 6, 2002; Revised Manuscript Received May 6, 2003

ABSTRACT: Thermal annealing of organic light-emitting diodes based on polymer composites prior to the metal deposition is found to substantially improve the devices' luminescence efficiency. Phase separation between the matrix polymer and the hole conducting low molecular weight component is shown to be the origin of this behavior. We use atomic force microscopy along with selective dissolution of one of the components to establish the domain morphology of the devices. The presence of the metal electrode is shown to significantly influence the phase separation process. Finally, a correlation between the domain morphology and the electrooptical properties is established.

1. Introduction

The behavior of polymer blends confined to thin films has been studied extensively throughout the past decade both experimentally[1−4] and theoretically.[5−7] Meanwhile, a comprehensive knowledge has accumulated on how external interfaces can influence the phase behavior and the morphology formed during phase separation. While most of this knowledge came about from studies of model polymer blends, practical implications of what is often referred to as surface directed phase separation have only rarely been discussed.[8−11] This is partly due to the fact that technologically relevant blend systems tend to be more complex and less well-defined than model systems, thereby rendering systematic studies difficult if not impossible. However, polymer blend surfaces and thin films are indeed important in a variety of technological applications. Therefore, the transfer of the concepts from model systems to applications is an important and challenging task. The field of organic light-emitting devices (OLEDs) is a good candidate for such transfer. The field has rapidly grown in the past years,[12,13] and first applications have entered the market. Different functionalities such as charge injection, charge transport, or color and polarization tuning are typically provided by different materials that are either used in layered structures or as composites or in combinations of both.[14−20] Especially the composite systems are often thermodynamically unstable. There have been studies of polymer blend systems by Adachi et al.[21] The authors show that PMMA and PC-TPD phase separate already during spin-coating to form submicrometer-sized emission sites in the final device. Neher et al. used doped polyimide alignment layers to achieve polarized emission which also phase separate during preparation. The mechanical rubbing of the alignment layer gave detailed insight into the phase morphology.[22] Little is known, though, about the morphological influence on the device performance and even less on the thermal stability of the morphologies and subsequent degradation of the devices.[20,22]

Composite systems consisting of a polymer and a low molecular weight species are expected to show a weaker tendency to phase separation than polymer blends, as the incompatibility increases with the molecular weight of the components. Spin-coated films do therefore not necessarily phase separate during preparation. Furthermore, the low molecular weight component can act as a plasticizer and influence the phase separation kinetics.

In the present contribution, we study the phase morphology of a thin film organic light-emitting diode based on a low molecular weight hole conducting material blended with an inert polymer material. We have exposed a series of devices with varying dopant concentrations to elevated temperatures for different periods of time, and we have compared films with a free surface and films covered with a metal electrode. We demonstrate that this treatment increases the device efficiency. We also show that this effect is related to structural changes within the composite matrix.

2. Experimental Methods

Single-layer OLEDs were fabricated by spin-casting the active luminescent layer (EML) from chloroform solution (≈2000 rpm, 20 mg/mL) onto ITO-coated substrates (resistivity < 20 Ω/sq). The thickness was typically about 100 nm. The EML consisted of varying amounts of *N,N*′-diphenyl-*N,N*′-(3-methylphenyl)-1,1′-biphenyl-4,4′-diamine (TPD; Syntec GmbH; varied between 10 and 40 wt %), 0.5 wt % perylene as the luminescent molecule, and poly(methyl methacrylate) (PMMA; M_w = 15 000 g/mol) as an electrically inert polymer matrix. The devices were then subjected to vacuum in order to remove residual solvent. Calcium (100 nm) was evaporated as low work function cathode. The diode area defined by the cathode was 0.09 cm^2. The different OLED devices were then characterized by monitoring the $I-V$ characteristics and the electroluminescence intenstity. All preparation steps as well as the characterization were performed under an inert gas atmosphere. The heat treatment was carried out under vacuum conditions as well as under ambient conditions. No influence of the surrounding atmosphere on the phase morphologies has been observed.

[†] Universität Bayreuth.
[‡] Universität München.
[§] Present address: Institut für Physikalische Chemie, Universität zu Köln, Luxemburgerstr. 116, 50939 Köln, Germany.
[⊥] Present address: Polymaterials GmbH, Sudetenstrasse 5, D-87600 Kaufbeuren.
* To whom correspondence should be addressed. E-mail georg.krausch@uni-bayreuth.de.

10.1021/ma0259259 CCC: $25.00
Published on Web 06/06/2003

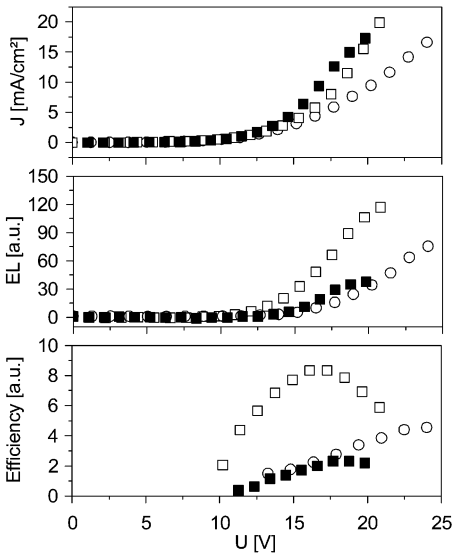

Figure 1. Characterization of devices of the general structure ITO/TPD(40 wt %):PMMA 100 nm/Ca. Voltage dependence of the current density (a), the electroluminescence output (b), and the efficiency (c) of a "regular" device (open circles), a "preheated" device (open squares), and a "postheated" device (solid squares).

The phase structure of the samples was investigated by scanning force microscopy (AFM). All AFM images were taken on commercial scanning force microscopes (Digital Instruments Multimode and Dimension 3100) operated in Tapping Mode. In some cases the samples were washed in cyclohexane to selectively remove the TPD domains from the sample. AFM images were taken at the same spot of the samples prior to and after thermal annealing or cyclohexane washing.

3. Results and Discussion

3.1. Optoelectronic Properties. Figure 1 shows the optoelectronic properties of OLEDs containing 40 wt % of TPD after exposure to different heating protocols. If the device is subjected to heat (100 °C, 5 min) prior to the deposition of the top electrode (open squares), the conductivity increases, as evident from the reduced current onset, the onset voltage for electroluminescence (EL) is lowered, and the efficiency is raised by up to a factor of 4 compared to the nontreated reference device (open circles). By contrast, if the thermal treatment is done after deposition of the electrode (filled squares), the conductivity also increases, but there is only a slight reduction of the EL onset voltage. The efficiency, though, remains more or less unchanged. Similar observations were obtained at lower TPD content, the main difference being an increase in both EL and current onset voltage with decreasing TPD content (not shown here) as has been reported before.[23] This effect can be attributed to the improved hole conductivity at higher TPD content.

3.2. Morphology. We have investigated the surface structure of the PMMA/TPD blend layers for different TPD concentrations. Together with results from selective dissolution experiments, these investigations can yield information about the domain morphology of the films. After spin-casting, the films exhibit an average roughness of about 1 nm independent of the TPD content. To simulate the aging process in OLEDs under operational conditions, the samples were heated to 100 °C for 5 min (akin the OLEDs; see above). The heating was performed on a hot plate under ambient conditions. The results of this procedure are shown in Figure 2 for

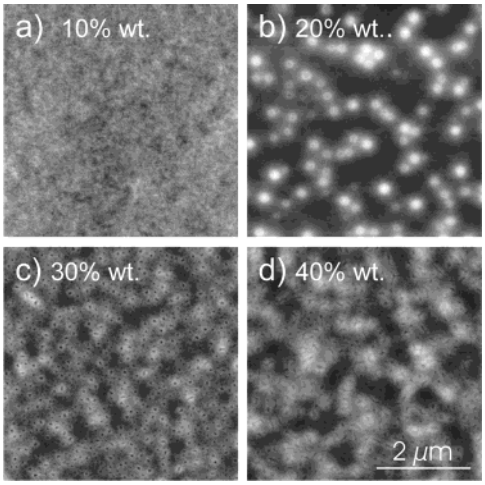

Figure 2. Topographic surface scans (5 × 5 μm) of samples containing various amounts of TPD dispersed in PMMA after heat treatment for 5 min at 100 °C: 10, 20, 30, and 40 wt % (height scales are 5, 20, 10, and 20 nm, respectively).

TPD concentrations ranging between 10 and 40 wt %. While the film surface remains relatively smooth for the lowest TPD concentration, characteristic changes of the film morphology are induced by the heat treatment at higher TPD content. For 20 wt % TPD, the film surface develops isolated protrusions, which are quite uniform in size (diameter: some 100 nm; height: some 10 nm). In addition, a few holes are observed in the film surface surrounded by a protruding rim. At higher TPD concentrations, the density of these protrusions increases, leading to a percolating elevated structure with small holes.

To understand the underlying process, we have studied the temporal evolution of the surface morphology for a TPD concentration of 24 wt % on a silicon substrate. No perlylene was added to the blend in these experiments as it was found to have no influence on the resulting structures. This finding indicates that at a concentration of 0.5 wt % perylene does not significantly affect the glass transition temperature of the blend and the overall phase separation process. In Figure 3A, we display a series of AFM images taken at the identical location of the sample after successive heating steps. Figure 3B shows cross sections of such images, the curves being shifted along the vertical axis for clarity. We find that the originally flat surface develops protrusions, which first tend to grow in height to about 10 nm and then expand laterally. At later stages of annealing, characteristic craterlike depressions are formed in the centers of the protrusions, which correspond to what was referred to as "holes" above. These depressions are only a few nanometers deep and do not deepen further on prolonged annealing. After the final heating step, the sample was immersed in cyclohexane. Being a selective solvent for TPD, cyclohexane is expected to remove potential TPD agglomerations located close to the surface. This treatment results in the formation of 30 nm deep craters around the center of each protrusion while the surface area in between the protrusions remains largely unaffected (the bottom curve in Figure 3B). As the bottom line of the craters is not clearly resolved in this experiment, the depth of the craters has been determined from additional experiments (not shown here). This finding indicates that the protrusions formed on annealing can be attributed to TPD agglomerations located in the vicinity of the sample

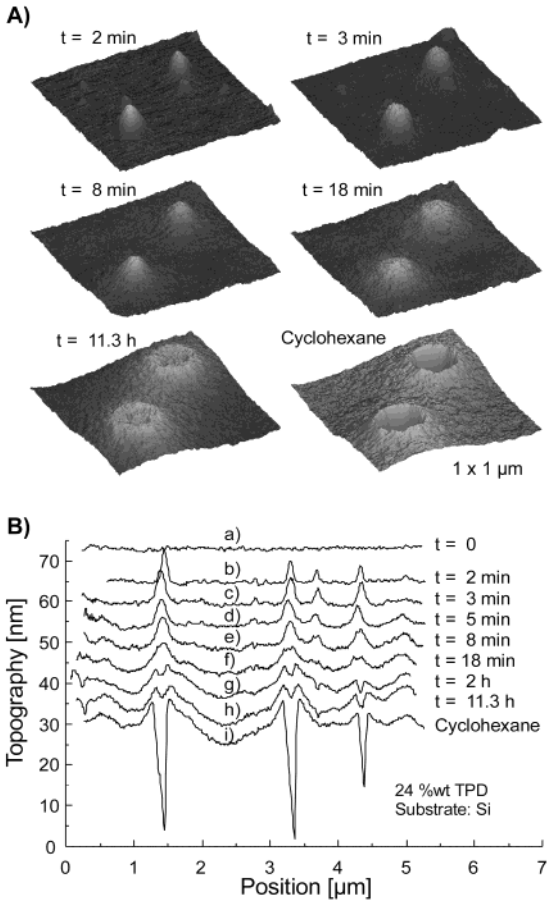

Figure 3. Cluster formation: morphological change of a sample containing 24 wt % of TPD dispersed in PMMA on a silicon substrate during heating. 3D views (A) and cross sections (B) of AFM images taken at (a) $t = 0$, (b) $t = 2$ min, (c) $t = 3$ min, (d) $t = 5$ min, (e) $t = 8$ min, (f) $t = 18$ min, (g) $t = 120$ min, and (h) $t = 680$ min are displayed. The individual cross-section curves are offset for clarity. The bottom-right image and the bottom-most curve show the topography after treatment with cyclohexane.

surface. Such agglomerations may result from phase-separation between PMMA and TPD. At higher TPD concentration, the AFM images indicate a bicontinuous domain morphology. We are led to assume that the TPD domains percolate into a continuous structure, which is still covered by a PMMA layer. Again, the same type of holes are observed in the PMMA layer.

We now turn in detail to the formation of these holes. The holes form during the early stages of annealing and do not grow in depth for longer times. To understand the origin of these features, it proves helpful to consider in some detail the shape of the cross sections through the TPD agglomerations after TPD removal in cyclohexane. The remaining PMMA surface is not flat but has formed wide rims around the TPD clusters (the bottom curve in Figure 3B). This is in agreement with studies of thin polymer blend films[24,25] where phase segregation leads to similar surface patterning upon annealing.[24,25] Karim et al. could show by secondary ion mass spectroscopy[24] that the droplet-forming component was covered by a thin layer of the matrix material.[24] In our case, the formation of the holes indicates a different situation: We assume that the clusters are originally completely covered by a thin PMMA layer which then ruptures and dewets from the TPD clusters as they grow in size and come closer to the surface.

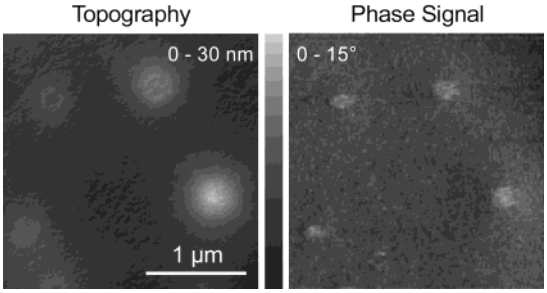

Figure 4. Topography and phase signal of a 24 wt % TPD/PMMA blend shortly after the rupture of the PMMA layer. The phase signal indicates a material contrast in the regions where a rim has formed. These regions are much smaller than the size of the protrusions, indicating that PMMA at this stage of the process still partially covers the TPD domains.

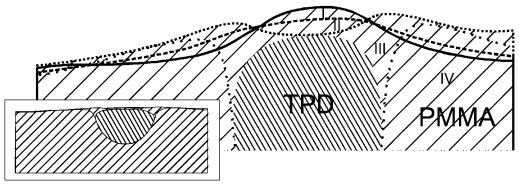

Figure 5. Sketch of the phase separation process for an uncovered composite film: (I) phase separation leads to TPD clusters that locally deform the film surface; (II) the surface deformation spreads further out; (III) dewetting of the PMMA from the TPD clusters; (IV) film morphology after selective dissolution of the TPD clusters. The inset shows the whole layer with the natural aspect ratio.

This notion is corroborated by tapping mode AFM experiments where the phase signal is simultaneously detected with topography (Figure 4): For freshly grown protrusions, the phase signal is laterally homogeneous, indicative of a homogeneous surface layer of a single component. With the hole formation, however, a significant phase contrast is observed between the inside of the holes and the rim. This finding strongly suggests that within the holes a free surface of TPD is formed. Obviously, the holes will not grow in depth beyond the thickness of the covering PMMA layer. Similar transient wetting has already been observed in thin films of other polymer blend systems.[26] A sketch of the morphology development is given in Figure 5.

As TPD can act as a plasticizer for PMMA, experiments at different TPD concentrations actually involve different mobilities in the polymer blend. To study the role of mobility changes, we have performed our experiments at different annealing temperatures between 60 and 120 °C (not shown here). The results indicate that the morphological changes are similar for all temperatures, while the kinetics of structure formation is naturally faster at higher temperatures. Furthermore, Figure 3 shows that the coarse-grained structure formed already after 5 min hardly changes on further annealing. Both findings lead us to the conclusion that the structures presented in Figure 2 are dominated by changes in composition rather than by changes in mobility.

For further investigation, experiments were performed on real OLED devices where the polymer film was partially covered with aluminum as cathode layer. We have used aluminum instead of calcium, as it was the only low work function metal that could be removed from the film without damaging it. No changes in the surface morphology of the cathode layer could be detected upon annealing. This finding is reasonable

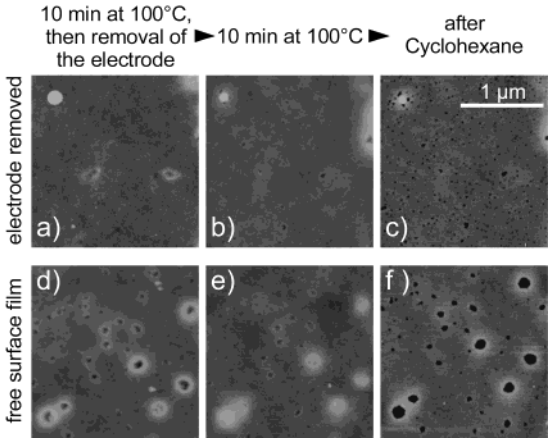

Figure 6. Comparison of the annealing process underneath an aluminum electrode (top) and in the close proximity of the electrode (bottom) for a sample containing 20 wt % of TPD dispersed in PMMA. Temporal evolution of the surface relief after $t = 10$ min (left, electrode was removed by immersing the device in water), after $t = 20$ min (middle), and after cyclohexane treatment (right). The height range is 20 nm for all images.

considering the small height of the protrusions observed on the free polymer surfaces (10 nm), the electrode thickness (100 nm), and the mechanical stiffness of the metal layer. After annealing, we removed the Al electrode by immersing the samples into water and investigated the surfaces (i.e., the original Al/polymer interface) by AFM. The result of this procedure is shown in Figure 6a−c together with images taken at a location that was not covered with aluminum (Figure 6d−f) for comparison. While protrusions and craters similar to the ones shown in Figure 3 have formed on the free polymer surface (Figure 6d), hardly any surface features are formed underneath the metal electrode upon annealing (Figure 6a). Even after cyclohexane treatment no changes of the film surface were observed (not shown here). More interestingly, though, a second annealing step performed after electrode removal leaves the surface rather smooth (Figure 6b) but leads to a similar hole formation as shown in Figure 6d, though on a smaller length scale and less pronounced. Immersion in cyclohexane then reveals a large number of small holes in the polymer surface, confirming the existence of numerous small TPD clusters (∼20 nm) in close proximity to the polymer surface (Figure 6c). These results indicate differences in the phase separation process between the uncovered and the metal-covered polymer film. In the originally uncovered area (Figure 6d−f), the second annealing step does not significantly alter the surface morphology, and immersion in cyclohexane results in the dissolution of large TPD clusters in agreement with the experiments discussed above.

If we assume that the presence of the metal electrode would suppress the phase separation between PMMA and TPD, the second annealing step (after electrode removal) should result in a surface morphology similar to the one formed after the first annealing step for the free polymer surface. A comparison of parts b and e of Figure 6 clearly demonstrates that this is not the case. Therefore, we are led to assume that phase separation has indeed taken place even underneath the electrode, however, in a distinctly different way compared to the uncovered polymer film. Obviously, the presence of the metal electrode suppressed the formation of large domains in the early stage of phase separation. Ade et al.[25] have shown that for thin films phase separation can be separated into three stages: initial phase separation, rapid coarsening, and coalescence. The understanding of the coarsening is that phase-separated domains rearrange in shape and lead to mass flow on a short time scale. Once separate domains have formed, further growth occurs on a larger time scale as it can only happen due to diffusion and coalescence. Thus, even the late stage of an annealed film still exhibits complex three-dimensional polymer/polymer interfaces. This leads us to the following interpretation of our results for the metal-covered films. The presence of the electrode prevents the rapid coarsening by suppressing the mass flow at the free surface. Nevertheless, initial phase separation and coalescence can still occur, leading to stable domains that are smaller in size than the ones observed in the uncoated films. However, the metal coating prevents them from reaching the free surface. The second annealing step (after removal of the top metal layer) leads to a dewetting from the TPD clusters so that the following cyclohexane treatment can selectively dissolve the TPD out of the film. The coalescence of domains for longer times, as described in refs 24 and 25, has not been observed explicitly in our experiments as we have not performed systematic experiments on very long time scales. (Annealing for 6 days at 100 °C did not produce any further change of the free surface films.) However, Figure 3A shows that coalescence does occur in the early stage of the phase separation process. Finally, another reason for not observing coalescence could be the fact that TPD acts as a plasticizer for PMMA, thus slowing down the coalescence process with progressing phase segregation.

In summary, the annealing process leads to the formation of TPD clusters separated by PMMA domains with a reduced TPD content. The diameter of the clusters is larger than the film thickness for uncoated films and smaller than the film thickness for metal-coated films. With this knowledge, we can interpret the electrooptical properties presented in section 3.1: The phase separation of PMMA and TDP leads to coherent current paths and thus increases the overall conductivity of the device, as observed. This is true for either heating protocols. In contrast, only the preheated devices show a change in efficiency. This means that a higher percentage of the injected charge carriers can radiatively decay. We recall that by preheating the TPD concentration at the surface is enhanced. Considering that for single-layer devices with a high hole mobility the recombination effectively happens at the cathode layer, we may speculate that the recombination probability at the cathode increases due to the higher TPD concentration at the cathode interface. In addition, the bigger size but smaller number of the TPD domains may improve the collision probability and thus the recombination of electrons and holes. This in turn would lead to an increased efficiency. We note that these results are similar to the findings of Carter et al. when mixing insulating oxide nanoparticles with the luminescent material.[27] However, the assumption that the increased efficiency is due to the suppression of current filaments seems inadequate for our experiments.

4. Conclusion

We have investigated the effect of thermal annealing on the morphology and performance of organic light-emitting diodes based on polymeric composites. We find

clear evidence for phase separation between the polymer matrix and the hole conductor. The phase separation process is strongly influenced by the presence of the top metal electrode. Both preheated and postheated devices show an increase in conductivity whereas only preheating of the films leads to an increase in efficiency. This is correlated to the change in the film morphology.

Acknowledgment. This work was supported by the Fonds der Chemischen Industrie, the State of Bavaria (Langfristprogramm Neue Werkstoffe), and the Deutsche Forschungsgemeinschaft (SFB 481).

References and Notes

(1) Jones, R. A. L.; Norton, L. J.; Kramer, E. J.; Bates, F. S.; Wiltzius, P. *Phys. Rev. Lett.* **1991**, *66*, 1326−1329.
(2) Bruder, F.; Brenn, R. *Phys. Rev. Lett.* **1992**, *69*, 624−627.
(3) Krausch, G. *Mater. Sci. Eng., R* **1995**, *14*, 1−94.
(4) Budkowski, A. *Interfaces Crystallization Viscoelasticity* **1999**, *148*, 1−111.
(5) Binder, K. *Adv. Polym. Sci.* **1999**, *138*, 1−89.
(6) Müller, M.; Binder, K.; Albano, E. V. *Int. J. Mod. Phys. B* **2001**, *15*, 1867−1903.
(7) Puri, S.; Frisch, H. L. *J. Phys.: Condens. Matter* **1997**, *9*, 2109−2133.
(8) Arias, A. C.; Corcoran, N.; Banach, M.; Friend, R. H.; MacKenzie, J. D.; Huck, W. T. S. *Appl. Phys. Lett.* **2002**, *80*, 1695−1697.
(9) Morgado, J.; Moons, E.; Friend, R. H.; Cacialli, F. *Adv. Mater.* **2001**, *13*, 810−814.
(10) Arias, A. C.; MacKenzie, J. D.; Stevenson, R.; Halls, J. J. M.; Inbasekaran, M.; Woo, E. P.; Richards, D.; Friend, R. H. *Macromolecules* **2001**, *34*, 6005−6013.
(11) Greczynski, G.; Kugler, T.; Salaneck, W. R. *Thin Solid Films* **1999**, *354*, 129−135.
(12) Friend, R. H.; Gymer, R. W.; Holmes, A. B.; Burroughes, J. H.; Marks, R. N.; Taliani, C.; Bradley, D. D. C.; Dos Santos, D. A.; Bredas, J. L.; Logdlund, M.; Salaneck, W. R. *Nature (London)* **1999**, *397*, 121−128.
(13) Heeger, A. J. *Solid State Commun.* **1998**, *107*, 673−679.
(14) Parker, I. D.; Pei, Q.; Marrocco, M. *Appl. Phys. Lett.* **1994**, *65*, 1272−1274.
(15) Wu, C. C.; Sturm, J. C.; Register, R. A.; Tian, J.; Dana, E. P.; Thompson, M. E. *IEEE Trans. Electron Dev.* **1997**, *44*, 1269−1281.
(16) Sainova, D.; Miteva, T.; Nothofer, H. G.; Scherf, U.; Glowacki, I.; Ulanski, J.; Fujikawa, H.; Neher, D. *Appl. Phys. Lett.* **2000**, *76*, 1810−1812.
(17) Miteva, T.; Meisel, A.; Knoll, W.; Nothofer, H. G.; Scherf, U.; Muller, D. C.; Meerholz, K.; Yasuda, A.; Neher, D. *Adv. Mater.* **2001**, *13*, 565.
(18) Baldo, M. A.; O'Brien, D. F.; You, Y.; Shoustikov, A.; Sibley, S.; Thompson, M. E.; Forrest, S. R. *Nature (London)* **1998**, *395*, 151−154.
(19) Lee, C. L.; Lee, K. B.; Kim, J. J. *Appl. Phys. Lett.* **2000**, *77*, 2280−2282.
(20) Grell, M.; Knoll, W.; Lupo, D.; Meisel, A.; Miteva, T.; Neher, D.; Nothofer, H. G.; Scherf, U.; Yasuda, A. *Adv. Mater.* **1999**, *11*, 671−675.
(21) Adachi, C.; Hibino, S.; Koyama, T.; Taniguchi, Y. *Jpn. J. Appl. Phys., Part 2: Lett.* **1997**, *36*, L827−L830.
(22) Meisel, A.; Miteva, T.; Glaser, G.; Scheumann, V.; Neher, D. *Polymer* **2002**, *43*, 5235−5242.
(23) Blochwitz, J.; Pfeiffer, M.; Fritz, T.; Leo, K. *Appl. Phys. Lett.* **1998**, *73*, 729−731.
(24) Karim, A.; Slawecki, T. M.; Kumar, S. K.; Douglas, J. F.; Satija, S. K.; Han, C. C.; Russell, T. P.; Liu, Y.; Overney, R.; Sokolov, O.; Rafailovich, M. H. *Macromolecules* **1998**, *31*, 857−862.
(25) Ade, H.; Winesett, D. A.; Smith, A. P.; Qu, S.; Ge, S.; Sokolov, J.; Rafailovich, M. *Europhys. Lett.* **1999**, *45*, 526−532.
(26) Straub, W.; Bruder, F.; Brenn, R.; Krausch, G.; Bielefeldt, H.; Kirsch, A.; Marti, O.; Mlynek, J.; Marko, J. F. *Europhys. Lett.* **1995**, *29*, 353−358.
(27) Carter, S. A.; Scott, J. C.; Brock, P. J. *Appl. Phys. Lett.* **1997**, *71*, 1145−1147.

MA0259259